Kelvin Waves around Antarctica

KAZUYA KUSAHARA AND KAY I. OHSHIMA

Institute of Low Temperature Science, Hokkaido University, Sapporo, Hokkaido, Japan

(Manuscript received 5 March 2014, in final form 11 August 2014)

ABSTRACT

The Southern Ocean allows circumpolar structure and the Antarctic coastline plays a role as a waveguide for oceanic Kelvin waves. Under the cyclic conditions, the horizontal wavenumbers and frequencies for circumpolarly propagating waves are quantized, with horizontal wavenumbers 1, 2, and 3, corresponding to periods of about 32, 16, and 11 h, respectively. At these frequencies, westward-propagating signals are detected in sea level variation observed at Antarctic coastal stations. The occurrence frequency of westward-propagating signals far exceeds the statistical significance, and the phase speed of the observed signal agrees well with the theoretical phase speed of external Kelvin waves. Therefore, this study concludes that the observed, westward-propagating sea level variability is a signal of the external Kelvin waves of wavenumbers 1, 2, and 3 around Antarctica. A series of numerical model experiments confirms that Kelvin waves around Antarctica are driven by surface air pressure and that these waves are excited not only by local forcing over the Southern Ocean, but also by remote forcing over the Pacific Ocean. Sea level variations generated over the Pacific Ocean can travel to the western side of the South American coast and cross over Drake Passage to the Antarctic continent, constituting a part of the Kelvin waves around Antarctica.

1. Introduction

The Kelvin wave is one of the fundamental waves in geophysical fluid dynamics and is involved in many atmospheric and oceanic phenomena on the Earth (LeBlond and Mysak 1978; Gill 1982; Holton 2004). The Kelvin wave is a type of gravity wave and is formed by the interaction of Earth's rotation and a lateral boundary. In the ocean, Kelvin waves are trapped against the coastline or the equator and propagate along these boundaries.

Because the Southern Ocean has no meridional boundary and allows circumpolar propagation, a solid boundary of the Antarctic continent can be considered a cyclic waveguide for oceanic Kelvin waves. This longitudinal cyclic condition of the Southern Ocean is unique in the global ocean. For circumpolarly propagating waves in the circumpolar domain, the horizontal wavenumber and the associated frequency should be quantized.

There are two kinds of oceanic Kelvin waves: internal and external. Until now, there have been numerous observational studies for internal Kelvin waves, which play substantial roles in a stratified coastal ocean. In contrast, regarding external Kelvin waves, which have a much larger scale and propagate much faster than internal Kelvin waves, the investigations have been very limited, except tidally generated external Kelvin waves (Platzman et al. 1981; Müller 2009).

Some previous modeling studies suggested that there are westward-propagating external Kelvin waves guided by the Antarctic continent (Platzman et al. 1981; Zahel and Müller 2005; Müller 2009). Platzman et al. (1981) calculated 56 normal modes for the global ocean in the period ranging from 8 to 80 h based on results of a finite-element barotropic numerical model and suggested that there exist Kelvin waves for wavenumbers 1, 2, and 3 around the Antarctic continent. The phase speed of external Kelvin waves at 4000-m depth is about 200 m s^{-1}. With this fast phase speed, the wavenumber-1 Kelvin wave takes about 30 h to circle the Antarctic coast; that is, the period of a normal mode associated with the wavenumber-1 Kelvin wave is about 30 h. Since the period of the normal mode is longer than those of main diurnal tides (O_1 is 25.82 h, and K_1 is 23.93 h), tides cannot be a major driving

Corresponding author address: Kazuya Kusahara, Institute of Low Temperature Science, Hokkaido University, N19W8, Kita-ku, Sapporo 060-0819, Japan.
E-mail: kazuya.kusahara@lowtem.hokudai.ac.jp

DOI: 10.1175/JPO-D-14-0051.1

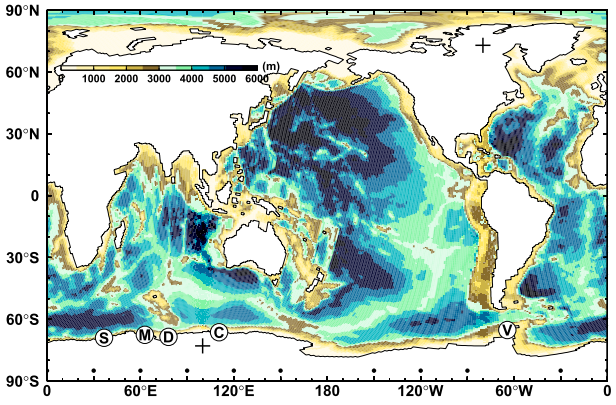

FIG. 1. Bottom topography in the numerical ocean model. Labels S, M, D, C, and V indicate Syowa, Mawson, Davis, Casey, and Vernadsky–Faraday stations, respectively. The crosses over the Antarctic continent and the Canadian Archipelago show locations of the two poles in the numerical model. Black dots over the Antarctic continent indicate longitudes used for depth profiles in Fig. 2a.

force for the wave in a linear wave framework. Ponte and Hirose (2004) found a broad spectral peak of sea level variations at around the period of 30 h in their numerical experiment that is driven by surface air pressure and concluded that the spectral peak is caused by the surface air pressure–driven, wavenumber-1 Kelvin wave around Antarctica. Furthermore, they calculated the phase relationship among three bottom pressure gauges in the Southern Ocean and showed that the phase difference among the gauges is explained by westward propagation of the wavenumber-1 Kelvin wave.

To our knowledge, only Ponte and Hirose (2004) offered the observational evidence of the external Kelvin wave around Antarctica. In principle, higher-wavenumber Kelvin waves are possible around Antarctica. Identification of higher-wavenumber Kelvin waves has not been made so far. Additionally, even for wavenumber 1, we have not understood the detailed characteristics of the Kelvin waves (i.e., occurrence frequency, seasonal variability, and main driving force). Kelvin waves around Antarctica should have maximum amplitude at the Antarctic coast. Therefore, sea level data observed at Antarctic coastal stations are expected to contain some signals of Kelvin waves. The purpose of this study is to assert the existence of external Kelvin waves from observed sea level data at several Antarctic stations (Fig. 1) and to investigate the characteristics and forcing mechanism, using a barotropic shallow-water ocean model.

2. External Kelvin waves in a circumpolar domain

In this section, we consider theoretical external Kelvin waves in a circumpolar domain. Since there is no meridional boundary, the Southern Ocean allows circumpolar features of waves and flows in the ocean. Under the cyclic boundary condition, the horizontal wavenumber k is quantized at integer values for circumpolarly propagating waves. The wavelength of the wavenumber-1 Kelvin wave ($k = 1$) corresponds to the circumpolar distance of the Southern Ocean (Lc $\approx$ 20 000 km at 60°S) and therefore the wavelength of higher wavenumbers ($k \geq 2$) is Lc/k. In the dispersion relation for Kelvin waves, there is a linear relationship between frequency and horizontal wavenumber; that is, the phase speed of Kelvin waves is independent of the horizontal wavenumber. Since the horizontal wavenumber for circumpolarly propagating waves is quantized, the frequency is also quantized. In this study, we call the quantized Kelvin waves trapped around the Antarctic continent Antarctic Kelvin waves (AKWs), following Ponte and Hirose (2004) and Müller (2009). Hereinafter, for convenience, the Antarctic Kelvin waves for wavenumbers 1, 2, and 3 are referred to as AKW1, AKW2, and AKW3, respectively.

Dispersion relations of Kelvin waves for several cross-shore bottom topographies are shown in Fig. 2b. We considered barotropic, f-plane (an assumption of the constant Coriolis parameter), linear, and inviscid motion for calculating the dispersion relation with the Coriolis parameter and the circumpolar distance at latitude 60°S. For simplicity, we assumed the uniformity of bottom topography in the alongshore direction. The cross-shore bottom topographies (Fig. 2a) were derived from the 5-minute gridded elevations/bathymetry for the world (ETOPO5); we subsampled every 30° longitude except the Weddell and Ross Seas (see black dots in Fig. 1 for the selected longitudes). We calculated the dispersion relation of the Kelvin waves for the mean bottom topography (thick red line in Fig. 2a), the deviated topography with one standard deviation (blue and green lines), and 4000-m flat topography (gray line) to examine sensitivity of the dispersion relation to changes in the bottom topography. A shooting method was used for calculating the dispersion relation and associated eigenfunctions of the Kelvin waves (Caldwell et al. 1972).

From the calculated dispersion relation (Fig. 2b), the phase speed of the AKWs is estimated to be 156–192 m s^{-1}. The quantized frequency bands correspond to the period range of 28.9–35.7, 14.5–17.9, and 9.6–11.9 h for the AKW1, AKW2, and AKW3, respectively. These period ranges of the AKWs rarely overlap the diurnal and semidiurnal tidal periods (22.31–28.01 and 11.61–13.17 h). Platzman et al. (1981) identified the three AKWs in their normal modes and estimated nominal Kelvin wave periods of 30.7, 15.3, and 10.2 h. These periods are consistent with the theoretical values of the AKWs frequency/period bands presented in this section.

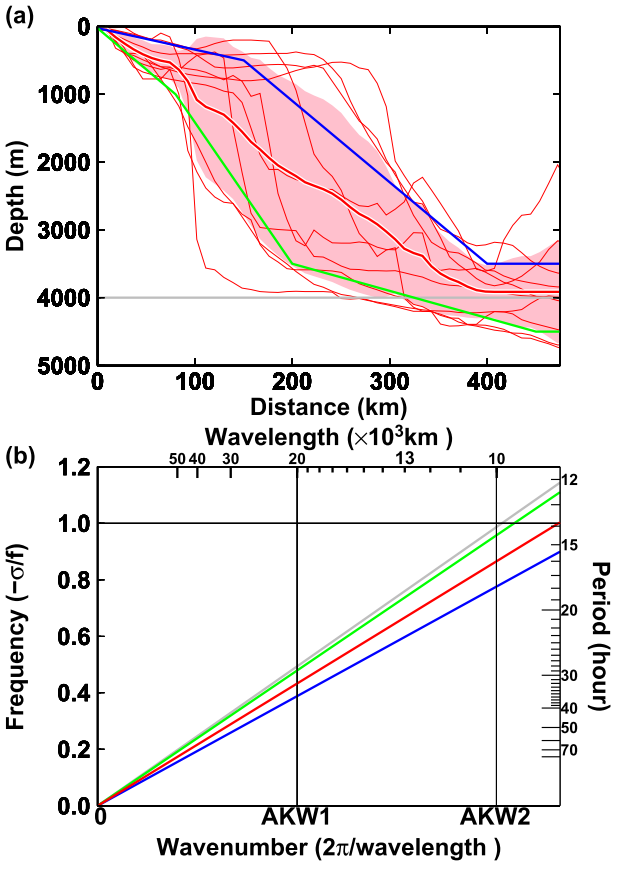

FIG. 2. (a) Depth profiles used for calculating the dispersion relation of the external Kelvin waves and (b) the dispersion relation. In (a), red thin lines indicate cross-shore bottom topographies subsampled every 30° except at the Weddell and Ross Seas (black dots in Fig. 1). The red thick line and shading show the mean topography and the deviated topography with one standard deviation, respectively. Blue and green lines indicate approximated profiles of the deviated topographies. The gray line shows 4000-m flat topography. The vertical axis σ in (b) is normalized with respect to the Coriolis parameter f. In (b), vertical thin lines indicate horizontal wavenumbers of the AKW1 and AKW2.

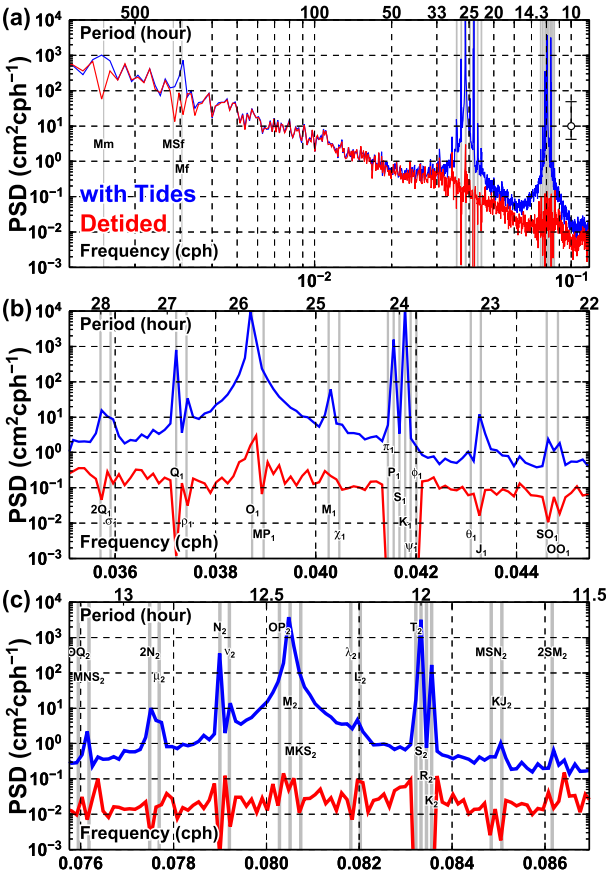

FIG. 3. Power spectra of coastal sea level with (blue) and without (red) tidal components for periods of (a) 8.5–900, (b) 22.0–28.5, and (c) 11.5–13.2 h. The spectra are averaged over the five stations and 3 yr. The horizontal axis indicates frequency, where a log scale is used for the top panel and a linear scale for the lower two panels. The error bar in the top panel is the 95% confidence level, where the equivalent degrees of freedom for the spectra are regarded as 3 (yr). The vertical gray lines indicate the tidal frequencies.

3. Observed Antarctic Kelvin waves

We used hourly sea level data at four stations [Syowa (69.0°S, 39.6°E), Mawson (67.6°S, 62.9°E), Davis (68.6°S, 78.0°E), and Casey (66.3°S, 110.5°E)] in East Antarctica and one station [Vernadsky–Faraday (65.3°S, 64.3°W)] on the western side of the Antarctic Peninsula. The locations of these Antarctic coastal stations are shown in Fig. 1. At these five stations, high-quality and long-term continuous records of coastal sea level are available (Aoki 2002; Hughes et al. 2003; Meredith et al. 2011). The sea level data for the time period from 1997 to 1999 were used for this study. The sea level was corrected for the inverse barometer effect, using the observed sea surface air pressure data; the air sea surface pressure data at the five stations were obtained from the Japan Oceanographic Data Center (for Syowa) and the British Oceanographic Data Centre (for the other four stations). The 60 components of tides were estimated by a conventional harmonic analysis using a least squares method (Emery and Thomson 2001) at each station in each year, and these tidal components were removed. Figure 3 shows the power spectra of the coastal sea level with and without the tides, confirming that the tidal components are leveled off in the detided sea level. In the following analyses, we utilized the hourly detided sea level data.

Figure 4 shows a Hovmöller diagram of sea level variations along East Antarctica (longitudes from 39° to 111°E) in 1998; a 25–40-h bandpass filter was applied to these time series. In this study the bandpass filter was designed by using Fourier and inverse Fourier transforms (Swarztrauber 1982). Westward-propagating signals exist throughout the year, although there are some periods

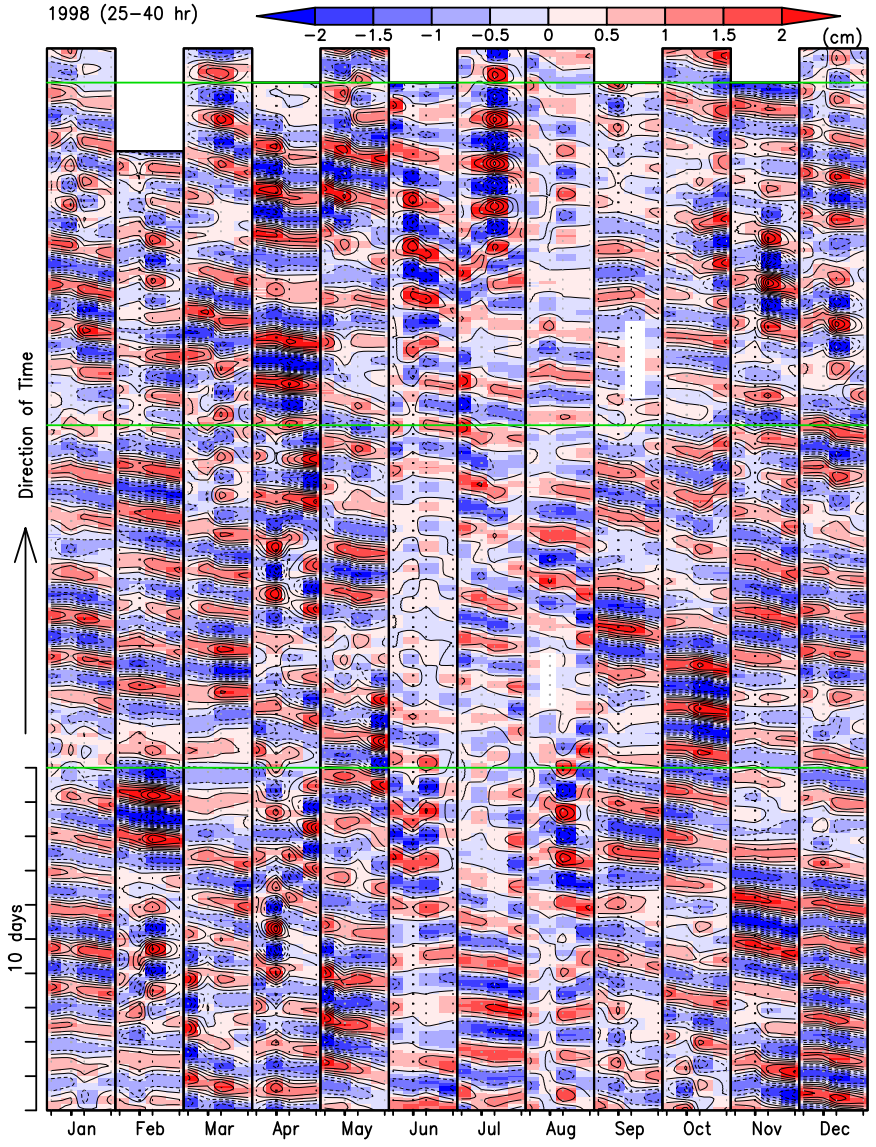

FIG. 4. Hovmöller diagram of sea level variation along the East Antarctic coast (39° to 111°E) for each month in 1998. The vertical black bars at the bottom indicate the longitudes of Syowa, Mawson, Davis, and Casey stations, from left to right for each month. A 25–40-h bandpass filter is applied to the sea level variations.

without apparent westward signals (i.e., the beginnings of February and April).

To examine the occurrence frequency of the westward-propagating signals, every 10 days we performed a frequency domain EOF (FDEOF; Wallace and Dickinson 1972) of the coastal sea level data around East Antarctica and examined the phase relationship among the four stations. The data at the Vernadsky–Faraday station were not used for the FDEOF analysis because there are a lot of short gaps in the time series. In the FDEOF analysis, we divided the sea level data into overlapping segments. The length of each segment is 128 h. The three consecutive segments that overlap 64 h with each other cover about a 10-day time period. Hereinafter, we call a combination of these three segments a ''data unit.'' We selected noon UTC on the fifth, fifteenth, and twenty-fifth of each month as the center of each data unit.

First, for each segment, the mean value was removed, and subsequently a Hanning filter was applied to reduce spectral leakage. Next, we calculated the cross-spectrum matrix, which consists of cross spectra for all combinations of the filtered sea level anomalies among the four stations. To increase statistical confidence, we averaged the cross-spectrum matrix over the frequency domain and

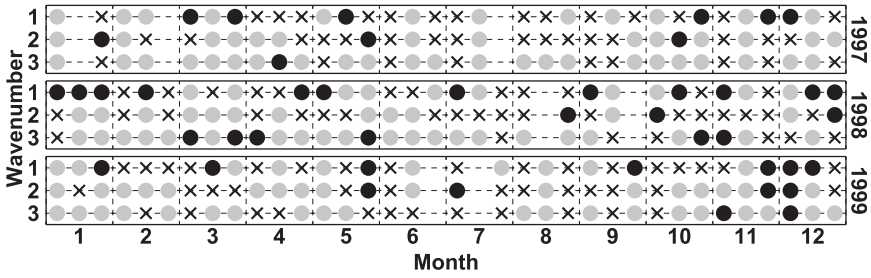

FIG. 5. Appearance calendar of the AKWs for the time period from 1997 to 1999. The vertical axis indicates the horizontal wavenumber (AKW1, AKW2, and AKW3). Circles (crosses) show the existence (or not) of westward-propagating signals based on the FDEOF of observed coastal sea level at four stations (see the text for details). No marks indicate missing periods of the analysis due to insufficient data. Among the circles, black ones indicate the time periods when the phase at all stations is within range of ±20° from the theoretical phase.

in the data unit. In this FDEOF analysis, signals with periods of 32.0 h are treated as the AKW1, those of 18.2, 16.0, and 14.2 h are treated as the AKW2, and those of 11.6, 10.7, 9.8, and 9.1 h are treated as the AKW3. Finally, we calculated the principal components in the averaged cross-spectrum matrix and estimated a phase relationship among the stations for each data unit (i.e., every 10 days).

Figure 5 shows a calendar of the occurrence frequency of westward-propagating signals in 1997, 1998, and 1999. The occurrence frequency was estimated from the phase relationship of the first FDEOF mode. In the calendar, circles indicate the time periods when the phase of all combinations of Syowa–Mawson, Mawson–Davis, and Davis–Casey exhibit westward propagation, otherwise crosses are placed. Black circles indicate the time periods when the phases at all the stations are within range of ±20° from the theoretical phase of the AKWs. The theoretical phase difference of the AKWs was calculated from the longitude and wavenumber, assuming that the Antarctic continent has a circumpolarly straight coastline at a constant latitude.

The westward-propagating signals of wavenumbers 1, 2, and 3 are found throughout the 3 yr, and there seems to be no seasonality in the occurrence frequency. Table 1 shows the number of the occurrence frequency of westward-propagating signals in each year and each wavenumber. It should be noted that the westward-propagating signals are detected with probability 0.125 even if all the signals are at random. The occurrence frequency of the observed, westward-propagating signals is higher than 9, which lies at the 99% significance level based on the cumulative distribution function of binomial distribution. Therefore, the observed westward-propagating signals along the Antarctic continent far exceed the statistical significance threshold.

Figure 6 shows the mean and standard deviation of the phase when the signals propagate westward. The phases are plotted relative to that at Casey station, and the theoretical phase propagation for the AKWs is also shown. For example, phase differences at Syowa station for wavenumbers 1, 2, and 3 are −84.7° ± 22.3°, −154.6° ± 21.1°, and −206.2° ± 27.8°, respectively. The phase differences estimated from the FDEOF analysis are consistent with the theoretical estimate of the AKWs. From these analyses, we confirm that the observed westward-propagating signals of sea level variation along the Antarctic coast indicate the AKWs in the real ocean. In the appendix, we show the cross spectra of the sea level data at the five stations, including Vernadsky–Faraday station, and confirm that westward-propagating signals are present circumpolarly around Antarctica, and the phase propagation is consistent with the AKWs.

4. Characteristics of Antarctic Kelvin waves

In the previous sections, we showed the existence of external Kelvin waves guided by the Antarctic continent by analyzing the observed coastal sea level and using simple linear wave theory. Here, a barotropic shallow-water ocean model was used to investigate in detail the characteristics of the AKWs and the driving force. We used the barotropic shallow-water model, because ocean stratification does not impact significantly on ocean circulation and sea level variation with a period shorter than a few days (Ponte and Vinogradov 2007).

a. Barotropic shallow-water model and numerical experiments

We used the barotropic shallow-water model in spherical coordinates, with a hydrostatic approximation and a horizontal resolution of 0.5° and 1° in the model's meridional and zonal directions, respectively. The model's poles were moved to the Canadian Archipelago (73°N, 80°W) and the East Antarctic continent (73°S, 100°E) to include the Arctic Ocean into the model domain, using the rotation

TABLE 1. Number of detections of westward-propagating signals along East Antarctic coast. Total number is the number of analysis period in each year. See also Fig. 5.

	1997	1998	1999
AKW1	18	22	17
AKW2	17	15	21
AKW3	24	27	22
Total number	33	34	34

of the coordinate system. A nonslip boundary condition was used for lateral boundaries. To model a spindown effect by the bottom Ekman layer, bottom friction was parameterized in a linear form as $-r\mathbf{u}/H$, with constant coefficient $r = 5.0 \times 10^{-4}\,\mathrm{m\,s^{-1}}$ (Chapman et al. 1986), where H is the ocean depth and $\mathbf{u}$ is depth-averaged horizontal velocity. Horizontal viscosity was parameterized in a Laplacian form, and its coefficient was set to a constant value of $5.0 \times 10^{3}\,\mathrm{m^2\,s^{-1}}$.

The wind stress was calculated from 6-hourly 40-yr European Centre for Medium-Range Weather Forecasts (ECMWF) Re-Analysis (ERA-40) wind data at 10-m height above the sea surface using a bulk formula (Trenberth et al. 1990). The existence of sea ice was ignored in the model. Bottom depth was derived from ETOPO5, and the model depth was smoothed by averaging the depth at each grid point and its four adjacent grid points. In the continental shelf regions adjacent to the Antarctic continent, grid points with depths shallower than 100 m were set as land points. Figure 1 shows the bottom topography of the model.

We performed a numerical integration for the time period from 1996 to 1999 and used the last 3 yr for this study. We conducted three numerical experiments driven by surface wind stress (W case), surface air pressure (P case), or surface wind stress and air pressure (WP case) to investigate the driving force of the AKWs. The surface boundary conditions derived from 6-hourly ERA-40 data were linearly interpolated to the model time step. For the following analyses, in the P and WP cases, we used the inverse barometer corrected sea level $\eta' = \eta - \eta^{\mathrm{IB}}$, where η is the sea level of prognostic variables in the model. The inverse barometer η^{IB} was calculated by $\eta^{\mathrm{IB}} = -(P_a - \overline{P_a})/(\rho g)$, where P_a is surface air pressure, $\overline{P_a}$ is the spatial average of the air pressure over the global ocean, ρ ($=1025\,\mathrm{kg\,m^{-3}}$) is a constant reference density, and g ($=9.8\,\mathrm{m\,s^{-2}}$) is gravitational acceleration.

b. Power spectra in the frequency domain

Power spectra of coastal sea levels at the East Antarctic stations from observation and numerical experiments (W, P, and WP cases) are shown in Fig. 7a. The spectra were estimated for each year and were averaged over the 3 yr and over 21 adjacent frequencies to increase the statistical confidence. The power spectra in the WP case

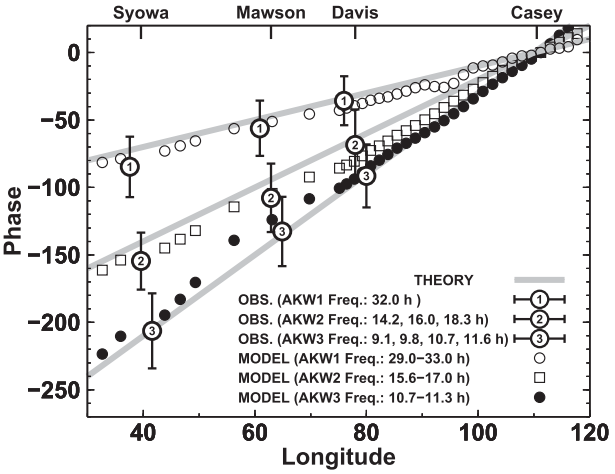

FIG. 6. Phase of sea level variation along the East Antarctic coast at AKW1, AKW2, and AKW3 frequencies. Relative phase differences from Casey station are plotted. Propagation of the phase is in the direction of decreasing phase. Results from observation, theory, and numerical model are shown by circles with error bars, gray lines, and symbols, respectively. The phase plots of AKW1 and AKW3 from the observation are slightly shifted in the longitudinal direction to avoid overlapping in the figure.

are roughly consistent with the observed ones in a wide frequency range (0.0025–0.11 cpd; period 9–400 h). In the P and WP cases, there are spectral peaks around periods of 25–40, 14–17, and 10–12.5 h. The peak around 25–40 h is consistent with the result of Ponte and Hirose (2004). In the observations, there are weak spectral peaks around periods of 30 and 11 h.

Next, we calculated a ratio of power spectra in the W and P cases to those in the WP case to investigate the main driving force for sea level variation with respect to each frequency. The sum of power spectra in the W and P cases approximately agrees with those in the WP case, implying that the Antarctic coastal sea level responds linearly to the two different forcings, at least in this model. The Antarctic sea level variation with the period shorter (longer) than 40 h is mainly driven by surface air pressure (surface wind stress). In other words, sea level variations with a period shorter than 40 h cannot respond statically to the surface air pressure. Since the periods of the AKWs are shorter than 40 h, surface air pressure is considered to be the main driving force of the AKWs. Note that Antarctic coastal sea level variation with a period longer than a few days is driven by wind stress (Fig. 7b) and that the coastal sea level variations fluctuate coherently around the Antarctic continent (Aoki 2002; Hughes et al. 2003; Kusahara and Ohshima 2009).

It should be noted that in Fig. 7, artificial signals with a 12-h period were removed by using a harmonic analysis. Without the removal, sharp spectral peaks appear at the period of 12 h in all the cases. We considered that these

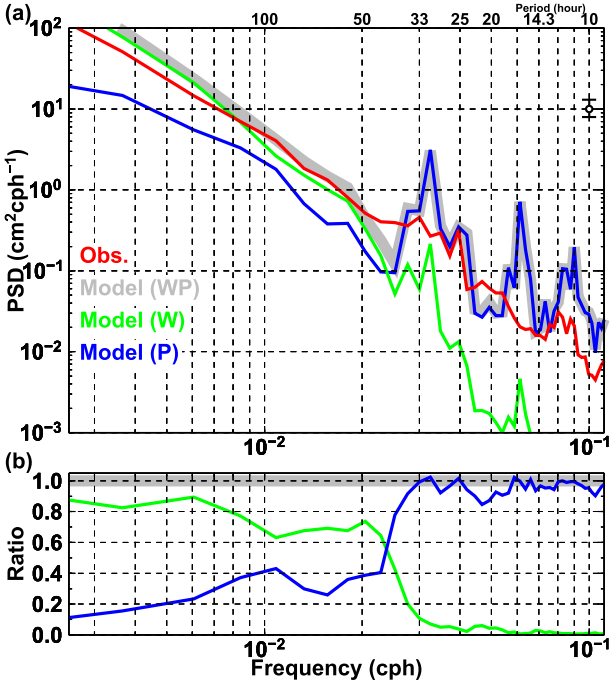

FIG. 7. (a) Power spectra of coastal sea level at four East Antarctic stations (Syowa, Mawson, Davis, and Casey). The spectra averaged over the stations are plotted. Red line indicates observed spectra. Gray, blue, and green lines indicate modeled results in the WP, W, and P cases, respectively. The error bar in the upper right is the 95% confidence level, where the equivalent degrees of freedom for the spectra are regarded as 3 (yr) × 21 (frequency bands). (b) Ratio of the power spectra in the W and P cases to those in the WP case.

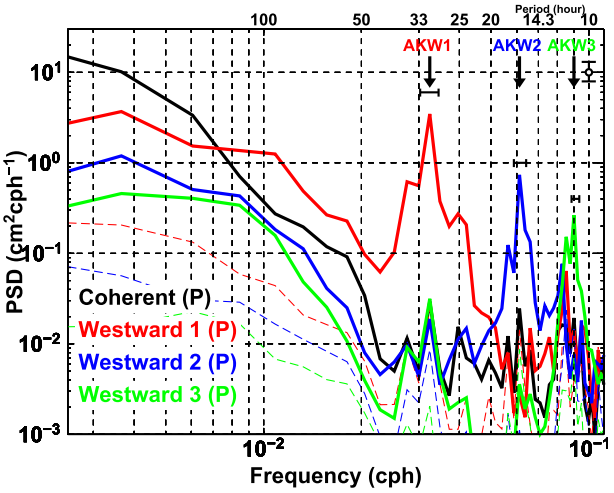

FIG. 8. Power spectra from space–time spectral analyses for coastal sea level in the numerical model. Red, blue, and green lines indicate horizontal wavenumbers 1, 2, and 3, respectively. Thick solid (thin dashed) lines indicate westward (eastward) components. Black line indicates the wavenumber-0 component. The error bar in the upper right indicates the 95% confidence level, the equivalent degrees of freedom for the spectra are set to 3 (yr) × 21 (frequency bands). The arrows indicate peak frequencies of the AKW1, AKW2, and AKW3. Horizontal bars indicate frequency bands used for the FDEOF analysis of the modeled sea level.

peaks are caused by the time resolution of 6 h in the surface boundary conditions.

c. *Power spectra in the frequency–wavenumber domain*

Space–time (frequency–wavenumber) spectral analysis (Hayashi 1971) was used to investigate the characteristics of Antarctic coastal sea level variation. This analysis is very effective for circumpolar phenomena like AKWs. The coastal sea level variation in the time–space domain can be expressed by the superposition of wavenumber-0, eastward- and westward-propagating components. For simplicity, we used the longitude of the coastal grid points in the space domain instead of distance along the Antarctic coast. Figure 8 shows the power spectra of the modeled sea level variation in the frequency–wavenumber domain. In the following analysis, we focus on signals with a period shorter than 40 h and mainly show the results of the P case since the WP case shows nearly identical results. The magnitudes of wavenumber-0 and eastward-propagating components are much smaller than those of westward-propagating components. Significant spectral peaks are present in the westward-propagating signals with the period of 29.0–33.0 h for wavenumber 1, 15.6–17.0 h for wavenumber 2, and 10.7–11.3 h for wavenumber 3. These periods of the spectral peaks are consistent with those of the AKWs.

d. *FDEOF of the modeled sea level*

To understand the spatial characteristics of the AKWs, FDEOF analysis was applied to the modeled sea level in the relevant frequency bands. In the FDEOF calculation for global-scale sea level variation, solving a large size complex eigenvector matrix is required. To reduce the computational cost, grid points in the model were subsampled at every five grid points in the horizontal directions and the mean of sea level averaged around the subsampled grid points were used for the FDEOF analysis in this subsection. Based on our estimation of the resonance frequencies of the AKWs in the model, we focus on the signals of the modeled sea level at three frequency bands, which corresponds to periods of 29.0–33.0, 15.6–17.0, and 10.7–11.3 h (indicated by horizontal bars in Fig. 8).

In all the three frequency bands, the AKWs are represented as a part of the principal mode of this FDEOF analysis (Fig. 9 for the AKW1), with the maximum amplitude at the Antarctic coast and westward propagation. The contributions of the principal modes are 86%, 56%, and 53% in the three frequency bands. The spatial

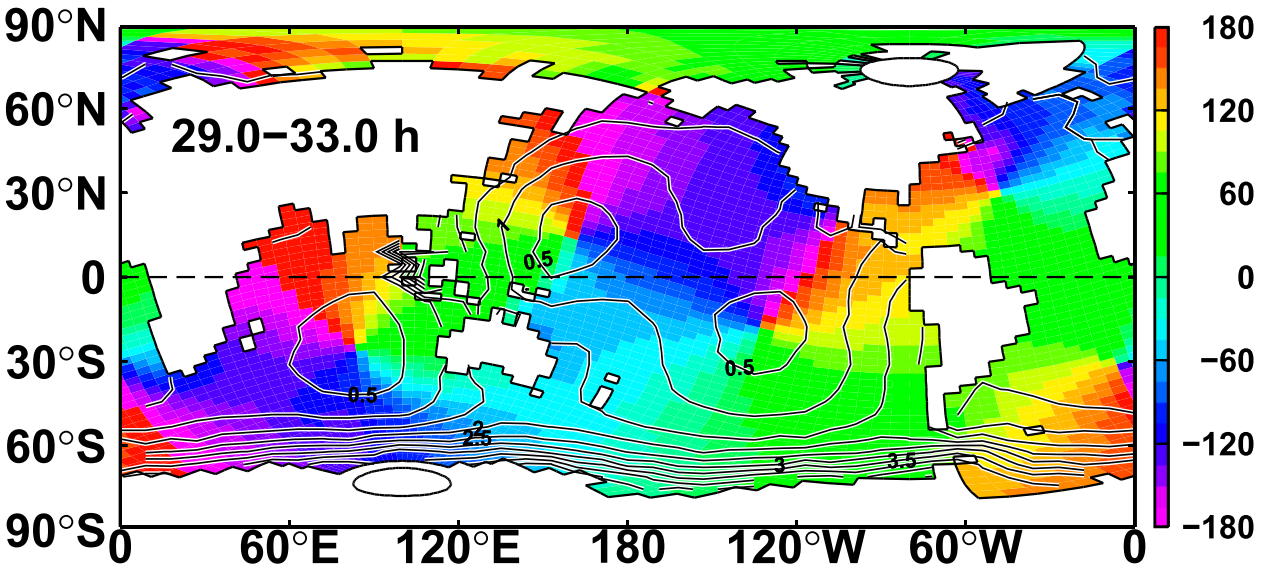

FIG. 9. Map of phase (shown by colors) and normalized amplitude (shown by contours) in the FDEOF analysis of modeled sea level variation at the periods of 29.0–33.0 h (AKW1). Propagation of the phase is in the direction of decreasing phase.

characteristics of the principal mode roughly correspond to the spatial patterns of normal modes of mode 16, mode 26, and mode 39 in Platzman et al. (1981). The phase of Antarctic coastal sea levels, which is estimated from this FDEOF analysis, is also overlaid on Fig. 6, showing good agreements among observations, model results, and the linear wave theory.

e. *Driving force*

From the numerical experiments forced by wind stress and/or surface air pressure, it is found that Antarctic coastal sea level variation with the period shorter than 40 h is mainly driven by surface air pressure (Fig. 7b). In this subsection, we investigate in detail which areas of the surface air pressure can drive the AKWs. We performed a series of numerical experiments in which region-confined anomalies of surface air pressure are used to force the ocean model. We subdivided the model domain into seven regions [indicated as Southern Ocean (SO), tropical Pacific Ocean (TP), North Pacific Ocean (NP), Indian Ocean (IO), tropical Atlantic Ocean (TA), North Atlantic Ocean (NA), and Arctic Ocean (AO) in Fig. 10]. A Gaussian function was applied to surface air pressure anomalies to smoothly connect from the forced region to unforced regions. This treatment was made to reduce the effect of discontinuous transition of forcing at the boundaries. It should be noted that the sum of surface air pressure anomalies in these numerical experiments does not coincide with the air pressure anomaly in the original P case owing to the use of the Gaussian function.

Figure 11 shows the ratio of the wavenumber–frequency power spectra of the seven experiments with region-confined forcing at the peak frequencies of the AKWs (see arrows in Fig. 8). The ratio is shown as relative contribution against the sum of power spectra of the seven experiments. The forcing in the Southern Ocean (SO case) contributes dominantly to Antarctic coastal sea level variations at all the AKWs frequencies, followed by the forcing in the North Pacific Ocean (NP case) and the tropical Pacific Ocean (TP case). Sea level anomalies generated by surface air pressure over the equatorial and North Pacific Oceans can propagate from the forced

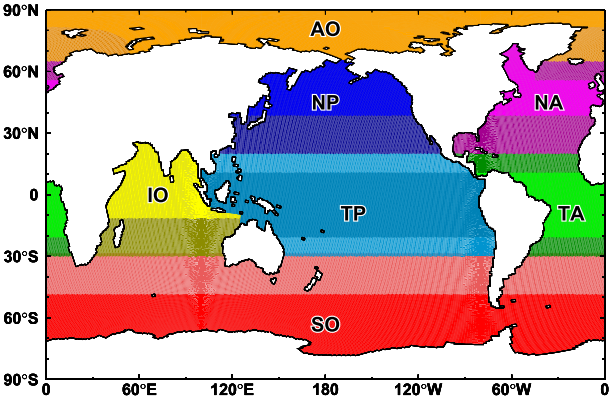

FIG. 10. Map of areas where a sea surface pressure anomaly is applied in the region-confined numerical experiments. Slightly changed color areas near the boundaries are regions where the pressure anomaly is gradually reduced to zero toward the boundary by a Gaussian function. SO indicates the Southern Ocean (red), TP is the tropical Pacific Ocean (light blue), NP indicates the North Pacific Ocean (dark blue), IO is the Indian Ocean (yellow), TA is the tropical Atlantic Ocean (green), NA is the North Atlantic Ocean (purple), and AO indicates the Arctic Ocean (orange).

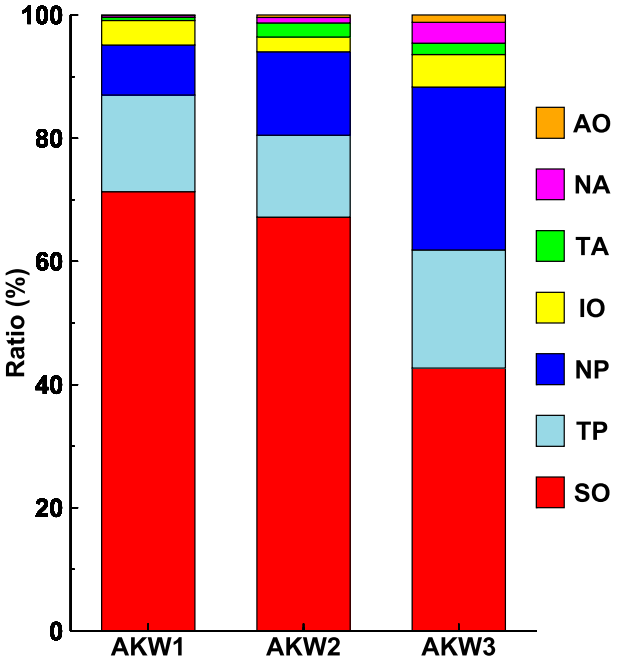

FIG. 11. Ratio of the power spectra of the seven numerical experiments with region-confined forcing for AKW1, AKW2, and AKW3 (see the text for details). See Fig. 10 for the regions of the confined forcing. See Fig. 8 for the spectral peak frequencies of the AKWs.

regions to the western side of South America through the equatorial Pacific as the external equatorial Kelvin waves, identified by the decreasing phase along this path in Fig. 9. Note that the equatorially trapped scale in Fig. 9 roughly corresponds to the external equatorial Rossby radius. Subsequently the signals propagate southward as the coastal Kelvin waves along the western side of the South American coast and finally reach the western side of the Antarctic Peninsula. The signals of Kelvin waves can jump and propagate to the Antarctic coast from the western side of South America because the width of the Drake Passage (about 650 km) is smaller than the external Rossby radius (about 1500 km). Since the cross-channel widths are much larger than the Rossby radius at the other choke points (i.e., south of Africa and Australia), the signals from the Indian and Atlantic Oceans cannot reach the Antarctic coast. Thus, the total contribution of sea level generated in these regions (IO, TA, NA, and AO) is small at all frequencies (less than 12%).

5. Summary and discussion

We have addressed external Kelvin waves around Antarctica from theoretical, observational, and numerical modeling perspectives. We have detected westward-propagating signals of wavenumbers 1, 2, and 3 from the Antarctic coastal sea level data (Figs. 4, 6, A2), with the occurrence frequency being statistically significant (Fig. 5; Table 1). Numerical experiments in which the shallow-water model is forced by wind stress and/or surface air pressure confirmed that the Antarctic coastal sea level variations with the period shorter than 40 h are mainly driven by surface air pressure (Fig. 7b). Phase speeds of the westward-propagating signals in the observation and numerical model agree well with the theoretical value of the external Kelvin waves (Fig. 6).

Since the Southern Ocean has no meridional boundary, the horizontal wavenumbers and frequencies of the circumpolarly propagating Kevin waves are quantized. It can be theoretically estimated that the frequencies for wavenumbers 1, 2, and 3 correspond to periods of 28.9–35.7, 14.5–17.9, and 9.6–11.9 h, respectively (Fig. 2). We have used the term Antarctic Kelvin waves (AKWs) to describe the quantized external Kelvin waves around Antarctica.

Spectral analysis of modeled coastal sea level variation in the frequency–wavenumber domain clearly shows the existence of westward-propagating waves, that is, the AKWs (Fig. 8). A series of numerical experiments forced by region-confined surface air pressures illustrates that the local surface air pressure over the Southern Ocean is the major contributor to the AKWs, while the remote forcing over the Pacific Ocean also contributes to the AKWs to some extent (Fig. 11). Sea level fluctuations excited over the equatorial and North Pacific Oceans can travel from the forced regions to the western side of South America as the equatorial Kelvin waves and subsequently can traverse the Drake Passage to the Antarctic continent (Fig. 9), partly constituting the AKWs (Fig. 11).

We detected signals of AKWs from sea level data observed at Antarctic coastal stations and estimated the occurrence frequency of westward-propagating signals and the phase relationship (Figs. 4, 5, 6). The occurrence frequency of westward-propagating signals far exceeds the statistical significance threshold (Fig. 5; Table 1), and the phase relationship of Antarctic coastal sea level variations is consistent with the theoretical phase propagation of the AKWs (Figs. 6, A2). This result strongly supports the existence of the AKWs in the real ocean and the previous findings in modeling studies (Platzman et al. 1981; Ponte and Hirose 2004). Particularly, we have clarified the existence of higher-wavenumber AKWs (AKW2 and AKW3) from observed sea level data for the first time.

From observations, AKW-like signals are not always present, and the appearance periods seem to occur at random with no seasonality (Fig. 5). In contrast, AKWs are always present in the numerical model (Fig. 7). The

difference between the occurrence in the observations and the numerical model probably arises both from quality of observed sea level data and unresolved physical processes in the numerical model. Since we have used sea level data only from 4 to 5 stations, mainly in East Antarctica, for detecting circumpolarly propagating signals, some noise even at one or a few stations in a certain period would prevent the detection of westward-propagating signals, even if there are AKWs in reality. Regarding the numerical modeling, there may be some uncertainties of representations of subgrid-scale dissipation processes and bottom friction, possibly leading to underestimation of dissipation in the numerical model.

The time resolution of surface boundary conditions (forcings) is also problematic for our modeling. In this study, the 6-hourly surface boundary conditions of wind stress and surface air pressure are linearly interpolated to the model time step. This time resolution is sufficient for the AKW1 whose period is about 30 h, while not for higher-frequency signals of AKW2 and AKW3. To better represent the higher-frequency signals, finer time resolution (about 1 h) would be required for surface boundary conditions.

The amplitudes of the AKWs at the Antarctic coast are about 1–2 cm (Fig. 4). It should be noted that observed amplitudes of diurnal and semidiurnal tides are ~30 cm (Fig. 3) and thus are much larger than those of the AKWs caused by the surface air pressure.

It is known that sea level variation at the Antarctic coast is strongly related to transport of the Antarctic Circumpolar Currents (ACC) and is sometimes used for the proxy for the ACC variability (Hughes et al. 1999). However, it should be kept in mind that the Antarctic coastal sea level variation also reflects the high-frequency coastal processes, as pointed out in this study and Kusahara and Ohshima (2009), as well as the long-term and large-scale oceanic variability.

High-frequency sea level variability discussed in this study presents a likely cause of aliasing of sea level data obtained from satellite altimeters, which globally measure the sea level height over several days. A numerical model that accurately represents high-frequency sea level variability, such as the model of Carrère and Lyard (2003), would be very useful for removing high-frequency signals and thus leaving behind the lower-frequency sea level variability.

In this study, we have focused on sea level variation with a period shorter than 40 h and demonstrated the existence of the AKWs in the real ocean and its characteristics. Long-term and high-quality observations at several Antarctic coastal stations allow us to detect such very high-frequency signals. Antarctic coastal sea level data have been used for monitoring the long-term Southern Ocean system. In addition, the high-quality dataset is also very useful for fundamental and classical geophysical fluid problems, as demonstrated in this study.

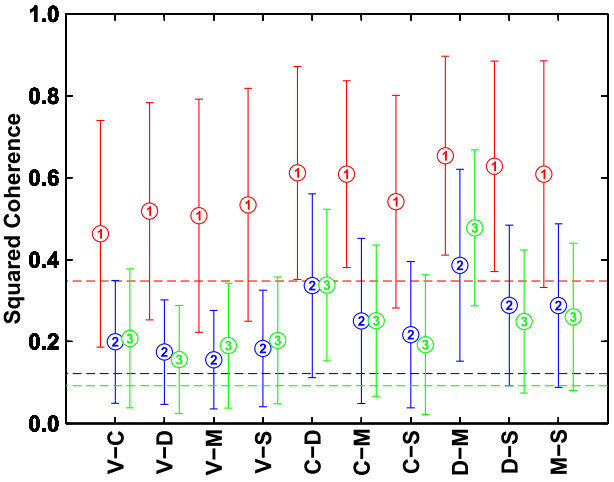

FIG. A1. Squared coherence for the frequencies of AKW1 (red), AKW2 (blue), and AKW3 (green) in sea level variation between two stations. The average (numbered circles) and one standard deviation (color error bars) of the results from all the data units of the approximate 10-day period are shown. The horizontal axis indicates combinations of two stations. Labels S, M, D, C, and V represent Syowa, Mawson, Davis, Casey, and Vernadsky–Faraday stations, respectively. Horizontal dashed lines indicate the 95% confidence levels. The equivalent degrees of freedom for the spectra of AKW1, AKW2 and AKW3 are $^{8}/_{3}$ (Hanning filter) × 3 (data segments) × 1 (frequency bands), $^{8}/_{3} \times 3 \times 3$, and $^{8}/_{3} \times 3 \times 4$, respectively.

Acknowledgments. We thank Dr. A. D. Fraser for his careful proofreading of the manuscript. This study was supported by Grant-in-Aids for Scientific Research A (25241001 and 26247080) and B (23340138) and the Research Activity Startup (25887001) from the Japan Society for the Promotion of Science (JSPS) and by the Canon Foundation. We are grateful to the two anonymous reviewers for their careful reading and constructive comments on the manuscript.

APPENDIX

Circumpolar Detection of Antarctic Kelvin Waves

Vernadsky–Faraday station, located on the western side of the Antarctic Peninsula, is far (more than 100° in longitude) from the other four East Antarctic stations. We did not use the sea level data at Vernadsky–Faraday station in the FDEOF analysis in the main text because there are many small data gaps. In this appendix, we

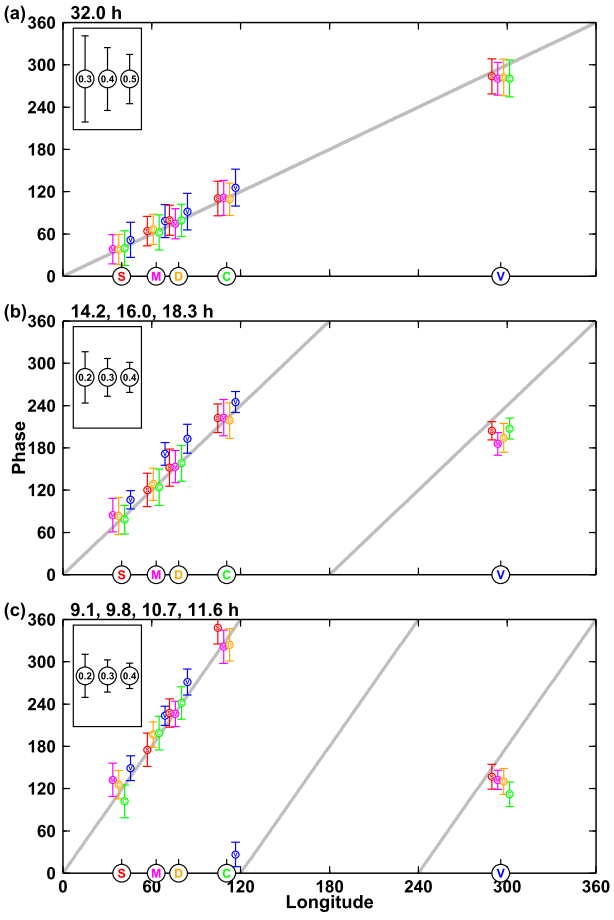

FIG. A2. Observed phase difference for the frequencies of (a) AKW1, (b) AKW2, and (c) AKW3 in sea level variation between each pair of two stations. The average (circles with letter) and one standard deviation (color error bars) of the results from all the data units of the approximate 10-day period are shown. Gray lines in (a),(b), and (c) show the theoretical phase lines of AKW1, AKW2, and AKW3, respectively. The phase at a station is calculated from the phase difference (estimated from the cross-spectra analysis) and the theoretical phase line of the other station of each pair (gray lines). Labels S, M, D, C, and V represent Syowa (red), Mawson (pink), Davis (yellow), Casey (green), and Vernadsky–Faraday (blue) stations, respectively. Plots of four pairs at a station are shifted slightly in the longitudinal direction to avoid overlapping in the figure. Error bars in the insets indicate 95% confidence level of the calculated phase difference for specified values (encircled number) of the squared coherence (Koopmans 1974).

show the result of the cross spectra (squared coherence and phase) of sea level variation between a pair of two stations including Vernadsky–Faraday station to confirm the circumpolar westward-propagating signals. The cross spectra are calculated for all possible combinations of two stations. Data preprocessing for the cross-spectra analysis is the same as that for the FDEOF analysis described in section 3 (size of the data segments, removing the mean sea level in each segment, applying the Hanning filter, and the frequency bands).

We calculated the squared coherences of all the two-station pairs for the frequencies of AKW1, AKW2, and AKW3. The calculation was made for all the data units of the approximate 10-day time period, and then the mean and standard deviation are presented in Fig. A1. The number of the data unit for the two-station pairs in the 3 yr is more than 100 in all the combinations. The confidence levels of the squared coherence (color dashed lines in Fig. A1) were estimated on the basis of the information of the data unit, where the equivalent degrees of freedom for the spectra of AKW1, AKW2, and AKW3 were set to $^{8}/_{3}$ (Hanning filter) $\times$ 3 (data segments) $\times$ 1 (frequency bands), $^{8}/_{3} \times 3 \times 3$, and $^{8}/_{3} \times 3 \times 4$, respectively. The mean of squared coherences exceeds the 95% confidence levels in all the pairs, indicating that there are rigid correlative signals for frequency bands of AKW1, AKW2, and AKW3. For these frequency bands Fig. A2 shows the mean phase difference of sea level for each pair from all the data units, when the squared coherence exceeds the 95% confidence levels. Note that the color error bars in Fig. A2 show one standard deviation of phase difference for all the data units of the pairs, and the black error bars in the insets show the 95% confidence level of the calculated phase difference for specified values (encircled number) of the squared coherence. The absolute phase of a station plotted in Fig. A2 is the relative phase difference on the theoretical phase line of the other station of each pair. The phase differences are highly consistent with the theoretical value for the AKWs. In addition to the FDEOF analysis in the main text, the results of the cross spectra in this appendix confirm that the external Kelvin waves around Antarctica for wavenumbers 1, 2, and 3 exist circumpolarly in the real ocean.

REFERENCES

Aoki, S., 2002: Coherent sea level response to the Antarctic Oscillation. *Geophys. Res. Lett.,* **29,** 1950, doi:10.1029/2002GL015733.

Caldwell, D. R., D. L. Cutchin, and M. S. Longuet-Higgins, 1972: Some model experiments on continental shelf waves. *J. Mar. Res.,* **30,** 39–55.

Carrère, L., and F. Lyard, 2003: Modeling the barotropic response of the global ocean to atmospheric wind and pressure forcing—Comparison with observations. *Geophys. Res. Lett.,* **30,** 1275, doi:10.1029/2002GL016473.

Chapman, D. C., J. A. Barth, and R. C. Beardsley, 1986: On the continuity of mean flow between the Scotian shelf and the Middle Atlantic Bight. *J. Phys. Oceanogr.,* **16,** 758–772, doi:10.1175/1520-0485(1986)016<0758:OTCOMF>2.0.CO;2.

Emery, W. J., and R. E. Thomson, 2001: *Data Analysis Methods in Physical Oceanography.* 2nd ed. Elsevier, 638 pp.

Gill, A. E., 1982: *Atmosphere–Ocean Dynamics.* Academic Press, 662 pp.

Hayashi, Y., 1971: A generalized method of resolving disturbances into progressive and retrogressive waves by space Fourier and time cross-spectral analyses. *J. Meteor. Soc. Japan,* **49,** 125–128.

Holton, J. R., 2004: *An Introduction to Dynamic Meteorology.* International Geophysics Series, Vol. 88, Elsevier Academic Press, 535 pp.

Hughes, C. W., M. P. Meredith, and K. J. Heywood, 1999: Wind-driven transport fluctuations through Drake Passage: A southern mode. *J. Phys. Oceanogr.,* **29,** 1971–1992, doi:10.1175/1520-0485(1999)029<1971:WDTFTD>2.0.CO;2.

——, P. L. Woodworth, M. P. Meredith, and V. Stepanov, 2003: Coherence of Antarctic sea levels, Southern Hemisphere annular mode, and flow through Drake Passage. *Geophys. Res. Lett.,* **30,** 1464, doi:10.1029/2003GL017240.

Koopmans, L. H., 1974: *The Spectral Analysis of Time Series.* Academic Press, 366 pp.

Kusahara, K., and K. I. Ohshima, 2009: Dynamics of the wind-driven sea level variation around Antarctica. *J. Phys. Oceanogr.,* **39,** 658–674, doi:10.1175/2008JPO3982.1.

LeBlond, P., and L. Mysak, 1978: *Waves in the Ocean.* Elsevier Oceanography Series, Vol. 20, Elsevier, 602 pp.

Meredith, M. P., and Coauthors, 2011: Sustained monitoring of the Southern Ocean at Drake Passage: Past achievements and future priorities. *Rev. Geophys.,* **49,** RG4005, doi:10.1029/2010RG000348.

Müller, M., 2009: *A Large Spectrum of Free Oscillations of the World Ocean including the Full Ocean Loading and Self-Attraction Effects.* Hamburg Studies on Maritime Affairs, Vol. 14, Springer, 118 pp.

Platzman, G. W., G. A. Curtis, K. S. Hansen, and R. D. Slater, 1981: Normal modes of the World Ocean. Part II: Description of modes in the period range 8 to 80 hours. *J. Phys. Oceanogr.,* **11,** 579–603, doi:10.1175/1520-0485(1981)011<0579:NMOTWO>2.0.CO;2.

Ponte, R. M., and N. Hirose, 2004: Propagating bottom pressure signals around Antarctica at 1–2-day periods and implications for ocean modes. *J. Phys. Oceanogr.,* **34,** 284–292, doi:10.1175/1520-0485(2004)034<0284:PBPSAA>2.0.CO;2.

——, and S. V. Vinogradov, 2007: Effects of stratification on the large-scale ocean response to barometric pressure. *J. Phys. Oceanogr.,* **37,** 245–258, doi:10.1175/JPO3010.1.

Swarztrauber, P. N., 1982: Vectorizing the FFTs. *Parallel Computations,* G. Rodrigue, Ed., 51–83, doi:10.1016/B978-0-12-592101-5.50007-5.

Trenberth, K. E., W. G. Large, and J. G. Olson, 1990: The mean annual cycle in global ocean wind stress. *J. Phys. Oceanogr.,* **20,** 1742–1760, doi:10.1175/1520-0485(1990)020<1742:TMACIG>2.0.CO;2.

Wallace, J. M., and R. E. Dickinson, 1972: Empirical orthogonal representation of time series in the frequency domain. Part I: Theoretical considerations. *J. Appl. Meteor.,* **11,** 887–892, doi:10.1175/1520-0450(1972)011<0887:EOROTS>2.0.CO;2.

Zahel, W., and M. Müller, 2005: The computation of the free barotropic oscillations of a global ocean model including friction and loading effects. *Ocean Dyn.,* **55,** 137–161, doi:10.1007/s10236-005-0029-y.